Stability analysis of thin film flow along a heated porous wall

Uwe Thiele,[1,a)] Benoît Goyeau,[2,b)] and Manuel G. Velarde[3,c)]
[1]*Department of Mathematical Sciences, Loughborough University, Leicestershire LE11 3TU, United Kingdom*
[2]*Laboratoire EM2C, UPR CNRS 288, Ecole Centrale Paris, Grande Voie des Vignes, F-92295 Châtenay-Malabry Cedex, France*
[3]*Instituto Pluridisciplinar, Universidad Complutense, Paseo Juan XXIII, n. 1, E-28040 Madrid, Spain*

(Received 8 May 2008; accepted 1 December 2008; published online 13 January 2009)

The time evolution of a thin liquid film flowing down a heated solid porous substrate is investigated. Using the Navier–Stokes and Darcy–Brinkman equations in the film and the porous layer, respectively, the problem is reduced to the study of the evolution equation for the free surface of the liquid film derived through a long-wave approximation. A linear stability analysis of the base flow is performed and the critical Reynolds and Marangoni numbers are obtained. A nonlinear analysis using continuation techniques shows that the base flow yields to stationary surface structures ranging from surface waves to large amplitude structures resembling sliding drops or ridges. It is also shown under what conditions the porous layer can be replaced by an effective slip boundary condition at the liquid-solid interface. Then, the corresponding slip length is calculated from the porous layer characteristics (thickness, porosity, and Darcy number). © *2009 American Institute of Physics*. [DOI: 10.1063/1.3054157]

I. INTRODUCTION

Liquid layers flowing on a solid wall and possessing a free surface can be described by a film thickness evolution equation obtained through a long-wave approximation of the Navier–Stokes equations.[1,2] Most works consider a smooth solid impervious substrate and therefore a no-slip and no-penetration boundary conditions for the fluid velocity at the fluid/substrate interface is adopted. In that case, Benney showed[3] that past a critical Reynolds number the base flow is unstable to a long-wave instability. However, Benney-type equations even with stabilizing surface tension have only a limited validity range since they lead to blow-up of solutions in finite time, which is not the case when solving the full Navier–Stokes equations.[4–7] On the other hand, it is known that a liquid layer resting on a heated smooth horizontal plate past a critical Marangoni number is unstable to either a short or to a long-wave Marangoni-driven instability.[8–13] In the latter case when the layer is really shallow film rupture and the emergence of dry spots is the result of instability if disjoining pressure and other molecular surface forces are not considered.[14–18] For a thin liquid film flowing on an inclined heated smooth solid wall with a Reynolds number of order unity, the above mentioned two long-wave instabilities may occur simultaneously.[19] For low enough Reynolds number flows only the long-wave Marangoni-driven instability survives. However, depending on the (small) inclination of the plate the final structures may exhibit small *or* large amplitude, e.g., surface waves or sliding drops, respectively.[17]

Actually, solid substrates are rarely smooth and they often are rather rough or even porous. Such situations are present in the (bio-)chemical, pharmaceutical, environmental, energy, and food industries. The objective of the present work is to study the influence of such permeable substrate on the stability of the liquid film flow. A pioneering study involving flow at a fluid-porous interface was performed by Beavers and Joseph.[20] The flows in the fluid and porous layers are described by the Stokes and Darcy equations, respectively, a semiempirical velocity slip boundary condition, justified theoretically by Saffmann,[21] was proposed at the interface. It involved a dimensionless slip coefficient which depends on the local geometry of the interface.[22] Recently, the magnitude of the slip velocity has been studied on an idealized porous wall[23] or for a fibrous porous structure.[24,25] However, the geometry of the interface is generally unknown and an alternative model consists in using the Darcy–Brinkman equation in the porous layer.[26,27] In this case, partial differential equations for each region are of the same differential order and continuity of both velocity and shear stress can be satisfied at the fluid-porous interface. Solutions are found to be similar to the one obtained by Beavers and Joseph, with an unknown parameter being the effective viscosity coefficient of the Brinkman correction term. Since the latter is only acceptable for high porosity values,[28,29] most of the relations for the effective viscosity have been generally found to be very close to Einstein's law for dilute suspensions.[30] Recently, the description of momentum transport at the fluid-porous interfacial region has been improved using a volume averaging method.[31,32] An interfacial stress jump condition was derived involving a new "adjustable" parameter that has been found to be related to spatial changes in the effective properties of the porous layer (permeability, porosity, etc.) at the interface.[33]

The fluid-porous substrate configuration occurs during spreading and imbibition of liquid films or drops on a

[a)]Electronic mail: u.thiele@lboro.ac.uk. URL: http://www.uwethiele.de.
[b)]Electronic mail: benoit.goyeau@em2c.ecp.fr.
[c)]Electronic mail: mvelarde@pluri.ucm.es.

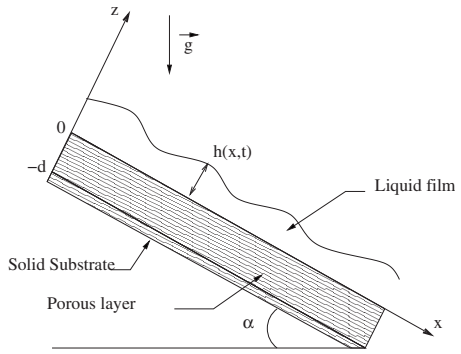

FIG. 1. Sketch of the two-dimensional geometry.

rough[34] or porous surface.[35,36] In both cases, continuity of pressure is imposed at the interface while boundary conditions for the velocity are described either by using the Beavers and Joseph slip condition[34] or by imposing continuity of velocity and shear stress.[35,36] A theoretical study has been performed in order to characterize the interface conditions for a thin film flow past a porous layer using Reynolds and Darcy equations in the film and the porous layer, respectively. Due to the nature of these equations, the coupling only provided a normal condition for the pressure at the interface.[37] Two stability analysis of fluid flow down a inclined isothermal porous surface have been previously performed.[38,39] In both cases, Darcy's law was used for momentum transport in the porous layer and therefore viscous diffusion at the interface is not included. The results that depend on the slip coefficient values show the destabilizing effect of the permeability.

As previously said, the objective of the present analysis is to study the influence of a heated porous substrate on the stability of the liquid film flow. The model is based on the Darcy–Brinkman equation in the porous substrate and a stress jump condition is imposed at the fluid-porous interface.

The paper is organized as follows. In Sec. II, the configuration is presented and the film thickness equation for a heated thin liquid film on an inclined porous substrate is derived. Limiting cases in terms of permeability, inclination, or Galileo number are discussed in Sec. III and a slip approximation model is also provided. Section IV is devoted to the linear stability analysis while fully nonlinear stationary solutions are studied in Sec. V. Special attention is focused on two limiting cases: an isothermal strongly inclined porous substrate and a heated slightly inclined or horizontal substrate. The salient results obtained are summarized in Sec. VI and possible applications, especially concerning the slip approximation, are pointed out.

II. FILM THICKNESS EQUATION

We consider a two-dimensional incompressible Newtonian liquid flowing over an inclined porous wall, saturated by the same liquid and heated from the side of the substrate (Fig. 1). Note that we consider a porous layer of a finite constant thickness d on a nonporous outer wall. The governing equations for mass, momentum, and energy balance in the liquid film are

$$\nabla \cdot \mathbf{u} = 0, \tag{1}$$

$$\rho(\mathbf{u}_t + \mathbf{u} \cdot \nabla \mathbf{u}) = -\nabla p + \mu \nabla^2 \mathbf{u} + \rho \mathbf{g}, \tag{2}$$

$$\rho c(T_t + \mathbf{u} \cdot \nabla T) = k_{\text{th}} \nabla^2 T, \tag{3}$$

where $\mathbf{u}$ represents the two-dimensional velocity field (u,w), p and T are the pressure and temperature fields, respectively, and $\mathbf{g}$ is the acceleration of gravity. In Eqs. (2) and (3), ρ, μ, c, and k_{th} stand for the density, viscosity, specific heat, and thermal conductivity of the fluid, respectively. In the following, buoyancy will be neglected since we consider sufficiently thin films. In Eqs. (2) and (3) and throughout the paper, partial derivatives are denoted by subscripts t, x, and z. The liquid flow inside the porous substrate is described using the Darcy–Brinkman equation[33,40,41]

$$\nabla \cdot \tilde{\mathbf{u}} = 0, \tag{4}$$

$$\frac{\rho}{b}\tilde{\mathbf{u}}_t = -\nabla \tilde{p} + \mu_{\text{eff}} \nabla^2 \tilde{\mathbf{u}} + \rho \mathbf{g} - \frac{\mu}{\kappa}\tilde{\mathbf{u}}, \tag{5}$$

where $\tilde{\mathbf{u}}$ is the filtration velocity vector $(\tilde{u},\tilde{w})$, κ is the permeability, b is the porosity, and μ_{eff} represents the effective viscosity. Following Whitaker,[42] the reduced viscosity is given by $\mu_{\text{eff}}/\mu = 1/b$. The flow in the porous region is assumed to be slow enough to neglect inertia.[43] Finally, local thermal equilibrium is considered in the porous layer and therefore, the energy balance is governed by the macroscopic equation

$$(\rho c)_{\text{eff}} \tilde{T}_t + (\rho c)\tilde{\mathbf{u}} \cdot \nabla \tilde{T} = k_{\text{th}}^{\text{eff}} \nabla^2 \tilde{T}, \tag{6}$$

where $\tilde{T}$ is the temperature, and $(\rho c)_{\text{eff}}$ and $k_{\text{th}}^{\text{eff}}$ are the effective volumic heat and the thermal conductivity of the medium, respectively.

The associated boundary conditions for the components of the velocity fields are the tangential and normal stress balance conditions at the free surface[44]

$$-(p - p_\infty)\mathbf{n} + 2\mu \underline{\mathbf{P}} \cdot \mathbf{n} = 2\sigma K \mathbf{n} + \nabla_s \sigma \quad \text{at} \quad z = h, \tag{7}$$

where $\underline{\mathbf{P}} = [\nabla \mathbf{u} + (\nabla \mathbf{u})^T]/2$ is the rate of the strain tensor, $\mathbf{n} = (-h_x, 1)/\sqrt{1 + h_x^2}$ is the unit normal vector, $\nabla_s = \nabla - (\mathbf{n} \cdot \nabla)\mathbf{n}$ is the surface gradient operator, and $K = -\frac{1}{2}\nabla \cdot \mathbf{n}$ is the mean curvature of the liquid-gas interface. Since the flow in the porous layer is governed by the Darcy–Brinkman equation, the momentum transport at the fluid-porous interface can be represented using the model proposed in Ref. 31 where the continuity of velocity

$$\tilde{\mathbf{u}} = \mathbf{u} \quad \text{at} \quad z = 0 \tag{8}$$

is combined with a shear stress jump condition given by

$$\mu_{\text{eff}} \tilde{u}_z - \mu u_z = \frac{\xi}{\sqrt{\kappa}} \tilde{u} \quad \text{at} \quad z = 0. \tag{9}$$

The jump coefficient ξ takes into account a spatial heterogeneity of the interfacial region. The jump condition, Eq. (9),

represents a *macroscopic* description of the momentum transport in a finite *mesoscopic* interfacial transition layer. The jump coefficient depends on the characteristics of the continuous spatial variations of the effective properties (porosity and permeability) in this transition layer.[33] It is of $O(1)$.

Equations (8) and (9) represent an improvement upon the slip boundary condition used by earlier authors.[34] The ideal homogeneous structure of the porous interface corresponds to $\xi=0$. Since in the present paper, the penetration flow into the porous substrate is small and slow, the jump condition only concerns the shear stress and continuity of normal stress at the interface is satisfied,

$$-\tilde{p}+2\mu_{\text{eff}}\tilde{w}_z=-p+2\mu w_z \quad \text{at} \quad z=0. \tag{10}$$

Note, however, that for strong and fast penetration flow into a porous medium it might be necessary to discuss such a jump. The question is not yet finally settled in literature. For recent results, see Ref. 45.

At $z=-d$ (interface of porous layer and smooth solid wall), no-slip and no-penetration conditions are imposed,

$$\tilde{\mathbf{u}}=0 \quad \text{at} \quad z=-d. \tag{11}$$

The boundary condition for the temperature at the free surface is given by Newton's cooling law

$$k_{\text{th}}\nabla T\cdot\mathbf{n}+\alpha_{\text{th}}(T-T_\infty)=0 \quad \text{at} \quad z=h, \tag{12}$$

where α_{th} is the heat transfer coefficient and T_∞ is the temperature of the air. Continuity of temperature and heat fluxes is satisfied at the fluid-porous interface

$$T=\tilde{T} \quad \text{at} \quad z=0, \tag{13}$$

$$k_{\text{th}}T_z=k_{\text{th}}^{\text{eff}}\tilde{T}_z \quad \text{at} \quad z=0, \tag{14}$$

while the temperature at the interface between the porous layer and the outer solid wall is

$$T=T_s \quad \text{at} \quad z=-d. \tag{15}$$

Finally, the liquid-gas interface is a material boundary where the velocity field obeys the kinematic condition

$$w-h_t-uh_x=0 \quad \text{at} \quad z=h. \tag{16}$$

This condition implies that the liquid-gas interface should remain always outside the porous medium (saturated porous layer).

The dimensionless form of the above equations and boundary conditions is obtained using the following dimensionless variables (with dashes):[8,46]

$$(x,z)=\left(\frac{\bar{h}}{\epsilon}x',\bar{h}z'\right), \quad (p,\tilde{p})=\frac{\mu^2}{\rho\bar{h}^2}(p',\tilde{p}'),$$

$$(u,\tilde{u})=\frac{\mu}{\rho\bar{h}}(u',\tilde{u}'), \quad (w,\tilde{w})=\epsilon\frac{\mu}{\rho\bar{h}}(w',\tilde{w}'), \tag{17}$$

$$t=\frac{\bar{h}^2\rho}{\mu\epsilon}t', \quad T'=\frac{(T-T_\infty)}{\Delta T},$$

where $\bar{h}$ is the mean thickness of the film and ϵ is the ratio of the length scales $\bar{h}/L\ll 1$, L denotes the characteristic length scale for a surface deformation, $\delta=d/\bar{h}$ is the dimensionless thickness of the porous substrate, and $\Delta T=T_s-T_\infty$ represents the temperature difference between the solid substrate and the ambient air.

Following Oron *et al.*[2] and Joo *et al.*,[19] the velocity scale ($U=U_1=\nu/\bar{h}$) is here related to kinematic viscosity $\nu=\mu/\rho$. Actually, due to the nature of the problem, a heated falling film, several velocity scales could be used: $U_2=\rho g\bar{h}^2\sin\alpha/\mu$ or $U_3=(\nu g\sin\alpha)^{1/3}$ related to gravity as flow agent (α being the inclination of the substrate from the horizontal), $U_4=(\partial\sigma/\partial T)(\Delta T/\mu)$ related to the Marangoni effect also as a flow agent, and the scale U_1 we use that is set by a material fluid property here the viscosity. We have chosen the latter as it plays neutral when comparing the action of gravity and the Marangoni effect which are the two major flow and instability agents here considered. Besides, the viscous scale has the advantage of embracing with no difficulty both large and small inclination limits. As a matter of fact, it can be shown that the above three different scales lead to practically the same mathematical problem. Under these circumstances, the dimensionless balance equations (after removing the dashes) in the liquid film are

$$0=u_x+w_z, \tag{18}$$

$$\epsilon(u_t+uu_x+wu_z)=-\epsilon p_x+\epsilon^2u_{xx}+u_{zz}+G\sin\alpha, \tag{19}$$

$$\epsilon^2(w_t+uw_x+ww_z)=-p_z+\epsilon^3w_{xx}+\epsilon w_{zz}-G\cos\alpha, \tag{20}$$

$$\epsilon\,\text{Pr}(T_t+uT_x+wT_z)=T_{zz}+\epsilon^2T_{xx}, \tag{21}$$

while in the porous layer they take the form

$$0=\tilde{u}_x+\tilde{w}_z, \tag{22}$$

$$\epsilon\frac{1}{b}\tilde{u}_t=-\epsilon\tilde{p}_x+\frac{1}{b}(\epsilon^2\tilde{u}_{xx}+\tilde{u}_{zz})-\frac{1}{\text{Da}}\tilde{u}+G\sin\alpha, \tag{23}$$

$$\epsilon^2\frac{1}{b}\tilde{w}_t=-\tilde{p}_z+\frac{1}{b}(\epsilon^3\tilde{w}_{xx}+\epsilon\tilde{w}_{zz})-\frac{\epsilon}{\text{Da}}\tilde{w}-G\cos\alpha, \tag{24}$$

$$\epsilon\,\text{Pr}(\Sigma\tilde{T}_t+\tilde{u}\tilde{T}_x+\tilde{w}\tilde{T}_z)=\Lambda_{\text{eff}}(\tilde{T}_{zz}+\epsilon^2\tilde{T}_{xx}), \tag{25}$$

where $\Sigma=(\rho c)_{\text{eff}}/(\rho c)$ and $\Lambda_{\text{eff}}=k_{\text{th}}^{\text{eff}}/k_{\text{th}}$. In these equations, $G=g\rho^2\bar{h}^3/\mu^2$ is the Galileo number, $\text{Pr}=\nu/\kappa_{\text{th}}$ is the Prandtl number, with $\kappa_{\text{th}}=k_{\text{th}}/\rho c$ the thermal diffusivity and $\text{Da}=\kappa/\bar{h}^2$ is the Darcy number representing the dimensionless permeability. Hence, the porosity is not necessarily related to the Darcy number and its influence on the stability of the film will be studied independently of the dimensionless permeability. Note that due to the chosen viscous scaling the Reynolds number takes the value unity ($\text{Re}=\rho\bar{h}U/\mu=1$) and hence it will not explicitly appear affecting inertia in the flow equations. The dimensionless parameters and their associated

TABLE I. Dimensionless numbers and their approximate values. Note that in the chosen "viscous scaling" the Reynolds number is equal to one.

Dimensionless group	Symbol	Physical interpretation	Definition	Approximate value
Aspect ratio	ϵ	$\frac{\text{mean film thickness}}{\text{lengthscale of surface structures}}$	$\frac{h}{L}$	10^{-2}
Bond number	Bo*	$\frac{\text{gravity}}{\text{curvature pressure}}$	$\frac{\mu^2 L^2}{\rho\sigma_0 \bar{h}^3}$	O(1)
Marangoni number	Ma	$\frac{\text{surface stress}}{\text{gravity}}$	$-\frac{\sigma_T \Delta T \rho h}{\mu^2}$	O(1)
Biot number	Bi	$\frac{\text{convective heat transfer}}{\text{conductive heat transfer}}$	$\frac{\alpha_{\text{th}} h}{k_{\text{th}}}$	O(1)
Prandtl number	Pr	$\frac{\text{viscous diffusion}}{\text{heat diffusion}}$	$\frac{\mu}{\rho}\frac{(\rho c)}{k_{\text{th}}}$	O(10)
Darcy number	Da	Dimensionless permeability	$\frac{\kappa}{\bar{h}^2}$	$0 \le \text{Da} \le \infty$
Porosity	b	Volume liquid fraction	$\frac{\mu}{\mu_{\text{eff}}}$	$0 < b < 1$
	Λ_{eff}	$\frac{\text{effective thermal conductivity}}{\text{thermal conductivity in the liquid}}$	$\frac{k_{\text{th}}^{\text{eff}}}{k_{\text{th}}}$	$O(1)$
	χ	Dimensionless stress jump coefficient	$\frac{\xi}{\mu}$	$O(1)$
	Σ	$\frac{\text{effective volumic heat}}{\text{volumic heat of the liquid}}$	$\frac{(\rho c)_{\text{eff}}}{(\rho c)}$	$O(1)$
Galileo number	G	$\frac{\text{inertia}}{\text{viscosity}}$	$\frac{g\rho^2 h^3}{\mu^2}$	$O(1)$

order of magnitude are summarized in Table I. The dimensionless boundary conditions at the free surface ($z=h$) and at the solid substrate ($z=-\delta$) are

$$[(u_z+\epsilon^2 w_x)(1-\epsilon^2 h_x^2)+2\epsilon^2(w_z-u_x)h_x] = -\epsilon \text{Ma}(T_x+h_x T_z)(1+\epsilon^2 h_x^2)^{1/2} \quad \text{at} \quad z=h, \tag{26}$$

$$-p-\frac{2}{1+\epsilon^2 h_x^2}[-\epsilon^3 u_x h_x^2-\epsilon w_z+\epsilon h_x(u_z+\epsilon^2 w_x)] = -\frac{\epsilon^2}{\text{Bo}}\frac{h_{xx}}{(1+\epsilon^2 h_x^2)^{3/2}} \quad \text{at} \quad z=h, \tag{27}$$

$$0=(\epsilon^2 h_x T_x-T_z)(1+\epsilon^2 h_x^2)^{-1/2}-\text{Bi}\,T \quad \text{at} \quad z=h, \tag{28}$$

$$w-h_t-uh_x=0 \quad \text{at} \quad z=h, \tag{29}$$

$$\tilde{\mathbf{u}}=0 \quad \text{at} \quad z=-\delta, \tag{30}$$

$$T=1 \quad \text{at} \quad z=-\delta, \tag{31}$$

while at the fluid-porous interface they take the form

$$\tilde{\mathbf{u}}=\mathbf{u} \quad \text{at} \quad z=0, \tag{32}$$

$$-\tilde{p}+2\frac{\epsilon}{b}\tilde{w}_z=-p+2\epsilon w_z \quad \text{at} \quad z=0, \tag{33}$$

$$\frac{1}{b}\tilde{u}_z-u_z=\frac{\chi}{\sqrt{\text{Da}}}\tilde{u} \quad \text{at} \quad z=0, \tag{34}$$

$$T=\tilde{T} \quad \text{at} \quad z=0, \tag{35}$$

$$T_z=\Lambda_{\text{eff}}\tilde{T}_z \quad \text{at} \quad z=0, \tag{36}$$

where the surface tension is assumed to vary linearly with temperature: $\sigma(T)=\sigma_0+\sigma_T(T-T_\infty)$. For most liquids, $\sigma_T<0$. The surface tension gradient was nondimensionalized using $\sigma_T\Delta T$. Therefore, the Marangoni number is $\text{Ma}=-\sigma_T\Delta T\rho\bar{h}/\mu^2$ while the Biot number is $\text{Bi}=\alpha_{\text{th}}\bar{h}/k_{\text{th}}$. In condition (34), $\chi=\xi/\mu$ is the dimensionless stress jump coefficient. Finally, $\text{Bo}=\mu^2/\rho\sigma_0\bar{h}$ compares the viscous normal stresses with surface tension. It is rescaled by $1/\epsilon^2$ (cf. Ref. 2), i.e., $\text{Bo}^*=\text{Bo}/\epsilon^2$.

Equations (18)–(25) with boundary conditions (26)–(36) are solved order by order in the smallness parameter ϵ. All fields (p, $\mathbf{u}$, $\tilde{\mathbf{u}}$, and T) and the time t are expanded as power series in ϵ as

$$\zeta=\zeta_0+\epsilon\zeta_1+O(\epsilon^2). \tag{37}$$

The explicit forms of order $O(1)$ and $O(\epsilon)$ are given in Appendix A. The equations for the velocity, pressure, and temperature in the liquid film *and* the porous substrate, Eqs. (A1)–(A3), (A5), and (A7) can be integrated directly, yielding

$$u_0=-\frac{G\sin\alpha}{2}z^2+C_0 z+C_1, \tag{38}$$

$$p_0=\tilde{p}_0=-G\cos\alpha z+C_2 \tag{39}$$

$$\tilde{u}_0 = \mathrm{Da}\, G \sin\alpha + C_3 e^{-\sqrt{b/\mathrm{Da}}\, z} + C_4 e^{\sqrt{b/\mathrm{Da}}\, z}, \tag{40}$$

$$T_0 = C_5 z + C_6, \tag{41}$$

$$\tilde{T}_0 = \frac{C_5}{\Lambda_{\mathrm{eff}}} z + C_6. \tag{42}$$

The velocity components normal to the substrate are determined using the corresponding continuity equations (A4) and (A8), giving

$$w_0 = -\frac{C_{0x}}{2} z^2 - C_{1x} z + C_7, \tag{43}$$

$$\tilde{w}_0 = C_{3x}\sqrt{\mathrm{Da}/b}\, e^{-\sqrt{b/\mathrm{Da}}\, z} - C_{4x}\sqrt{\mathrm{Da}/b}\, e^{\sqrt{b/\mathrm{Da}}\, z} + C_8. \tag{44}$$

The C_i with $i=0,\ldots,8$ are constants of integration that depend on the film thickness h and therefore on both the spatial coordinate x and time τ. They are determined using the boundary conditions (A9)–(A19) and are given in Appendix B. Using the results to $O(1)$ also the $O(\epsilon)$ Eqs. (A20) and (A22) can be integrated directly, yielding

$$\begin{aligned} u_1 = {} & \frac{1}{24}(C_0 C_{0x} + G \sin\alpha C_{1x}) z^4 \\ & + \frac{1}{6}(C_{0\tau} + C_{0x} C_1 - \mathrm{G} \sin\alpha C_7) z^3 \\ & + \frac{1}{2}(C_{2x} + C_{1t} + C_1 C_{1x} + C_0 C_7) z^2 + C_9 z + C_{10}, \end{aligned} \tag{45}$$

$$\begin{aligned} \tilde{u}_1 = {} & -\mathrm{Da}\, C_{2x} + \left(-\frac{1}{2}\sqrt{\frac{\mathrm{Da}}{b}} C_{3\tau} z + C_{11}\right) e^{-\sqrt{b/\mathrm{Da}}\, z} \\ & + \left(\frac{1}{2}\sqrt{\frac{\mathrm{Da}}{b}} C_{4\tau} z + C_{12}\right) e^{\sqrt{b/\mathrm{Da}}\, z}. \end{aligned} \tag{46}$$

The time derivatives of the constants obtained from $O(1)$ are all calculated using the $O(1)$ kinematic boundary condition (A19). Again the remaining velocity components w_1 and $\tilde{w}_1$ are obtained from continuity, Eqs. (A21) and (A23), respectively,

$$\begin{aligned} w_1 = {} & -\frac{1}{120}[(C_0 C_{0x})_x + G \sin\alpha C_{1xx}] z^5 \\ & - \frac{1}{24}[C_{0\tau x} + (C_{0x} C_1)_x - G \sin\alpha C_{7x}] z^4 \\ & - \frac{1}{6}[C_{2xx} + C_{1\tau x} + (C_1 C_{1x})_x + (C_0 C_7)_x] z^3 \\ & - \frac{1}{2} C_{9x} z^2 - C_{10x} z + C_{13}, \end{aligned} \tag{47}$$

$$\begin{aligned} \tilde{w}_1 = {} & \mathrm{Da}\, C_{2xx} z - \frac{1}{2}\sqrt{\frac{\mathrm{Da}}{b}}\left(\frac{\mathrm{Da}}{b} C_{3\tau x} - 2C_{11x} \right. \\ & \left. + \sqrt{\frac{\mathrm{Da}}{b}} C_{3\tau x} z\right) e^{-\sqrt{b/\mathrm{Da}}\, z} + \frac{1}{2}\sqrt{\frac{\mathrm{Da}}{b}}\left(\frac{\mathrm{Da}}{b} C_{4\tau x} - 2C_{12x} \right. \\ & \left. - \sqrt{\frac{\mathrm{Da}}{b}} C_{4\tau x} z\right) e^{\sqrt{b/\mathrm{Da}}\, z} + C_{14}. \end{aligned} \tag{48}$$

The C_i with $i=9,\ldots,14$ are constants of integration determined using the boundary conditions (A24)–(A28). They are given in Appendix B.

Introducing h_τ and h_{τ_1} [obtained from the corresponding kinematic boundary conditions, Eqs. (A19) and (A28)] we write

$$h_t = h_\tau + \epsilon h_{\tau_1} + O(\epsilon^2). \tag{49}$$

Thus the film thickness evolution equation is

$$\begin{aligned} h_t = {} & -\Gamma[F_1(h)]_x - \epsilon\left[\Gamma^2 F_2(h) h_x - \Gamma \cot\alpha F_3(h) h_x \right. \\ & \left. + \frac{\mathrm{Ma}^\star \mathrm{Bi}^\star}{(1+\mathrm{Bi}^\star h)^2} F_4(h) h_x + F_3(h)\frac{h_{xxx}}{\mathrm{Bo}^\star}\right]_x, \end{aligned} \tag{50}$$

where $\Gamma = G \sin\alpha$ is a modified Galileo number. Note that Γ can be seen as the Reynolds number corresponding to the velocity scale U_2. However, as we have chosen U_1 as velocity scale it is preferable to use a different name. The Reynolds number corresponding to the velocity scale U_1 is fixed to one as a result of the used scaling. The polynomial functions $F_i(h)$ are

$$\begin{aligned} F_1(h) &= \frac{h^3}{3} + r_1\frac{h^2}{2} + r_2 h, \\ F_2(h) &= \frac{2}{15} h^6 + r_3 h^5 + r_4 h^4 + r_5 h^3 + r_6 h^2 + r_7 h + r_8, \\ F_3(h) &= \frac{1}{3} h^3 + r_9 h^2 + r_{10} h + r_{11}, \\ F_4(h) &= \frac{1}{2} h^2 + r_{12} h + r_{13}. \end{aligned} \tag{51}$$

The expressions r_i are defined in Appendix B. In Eq. (50), $\mathrm{Ma}^\star$ and $\mathrm{Bi}^\star$ are *effective* Marangoni and Biot numbers, respectively,

$$\mathrm{Ma}^\star = \frac{\mathrm{Ma}}{1 + \mathrm{Bi}\dfrac{\delta}{\Lambda_{\mathrm{eff}}}}, \quad \mathrm{Bi}^\star = \frac{\mathrm{Bi}}{1 + \mathrm{Bi}\dfrac{\delta}{\Lambda_{\mathrm{eff}}}}. \tag{52}$$

Note that inertia (the convective terms) results in the term of Eq. (50) that goes with $F_2(h)$ making it a Benney-like equation.[3,7,19]

III. LIMITING CASES

Before performing the stability analysis it is pertinent to assess the behavior of Eq. (50) in some limiting cases.

A. Zero and infinite Darcy number

For very small values of the Darcy number ($\mathrm{Da}\to 0$), the porous medium behaves as a nonporous solid substrate. All the r_i in expressions (51) go to zero and only the highest order terms of the F_i remain. $\mathrm{Bi}^\star$ and $\mathrm{Ma}^\star$ rescale to Bi and Ma ($\Lambda_{\mathrm{eff}}\to\infty$), respectively, and Eq. (50) becomes

$$h_t = -\Gamma h^2 h_x - \epsilon\left[\frac{2}{15}\Gamma^2 h^6 h_x - \frac{1}{3}\Gamma\cot\alpha h^3 h_x + \frac{\mathrm{Ma\,Bi}}{(1+\mathrm{Bi}\,h)^2}\frac{h^2}{2}h_x + \frac{1}{3\mathrm{Bo}^\star}h^3 h_{xxx}\right]_x. \tag{53}$$

This film evolution equation corresponds to the one studied by Ref. 19 without evaporation and taking into account that here the factors 1/2 and 3 are not absorbed into the dimensionless numbers. For very large values of the Darcy number ($\mathrm{Da}\to\infty$), the porous layer behaves as a liquid layer (the porosity b goes to unity) with no-slip and no-penetration conditions at $z=-\delta$. The general form of Eq. (50) remains the same save changes in the constants r_i. Keeping b for the sake of later estimates one finds to highest order in 1/Da

$$\begin{aligned}
&r_1 = 2b\delta, \quad r_2 = b\delta^2,\\
&r_3 = \tfrac{4}{5}b\delta, \quad r_4 = \tfrac{1}{3}b(1+5b)\delta^2,\\
&r_5 = \tfrac{1}{3}b(1+4b+3b^2)\delta^3, \quad r_6 = \tfrac{1}{24}b(5+22b+24b^2)\delta^4,\\
&r_7 = \tfrac{1}{4}b^2(3+b)\delta^5, \quad r_8 = \tfrac{5}{24}b^2\delta^6,\\
&r_9 = b\delta, \quad r_{10} = b\delta^2,\\
&r_{11} = \tfrac{1}{3}b\delta^3, \quad r_{12} = b\delta,\\
&r_{13} = \tfrac{1}{2}b\delta^2.
\end{aligned} \tag{54}$$

Actually, the evolution equation in this limiting case should also be like Eq. (53) with a suitable film thickness $h+\delta$. Taking into account the necessary rescaling of Ma and Bi, and setting $b=1$ the new r_i fulfill this expectation for $i=1$, 2 and $i\geq 9$. Accordingly, the base flow and the hydrostatic, curvature pressure and Marangoni terms give the correct limit. However, inspecting r_3 to r_8 in Eq. (54) shows that the polynomial they form when introduced into Eq. (50) does not exactly correspond to $\frac{2}{15}(h+\delta)^6$. Indeed, the coefficients r_3-r_5 give the correct values (6, 15, and 20) while r_6-r_8 give approximately (15.9, 7.5, and 1.6) instead of the expected values (15, 6, and 1). Nevertheless, considering that this difference only exists for high order terms in δ the limit is still acceptable for $\delta\leq O(1)$. Note that this deviation rests on the use of the Darcy–Brinkman equation in the porous layer where nonlinear convective terms are not included. Therefore, for $\mathrm{Da}\to\infty$, the Darcy–Brinkman equation behaves as the Stokes equation.

B. Low values of the modified Galileo number $\Gamma = G\sin\alpha$

Two cases may be distinguished:

(i) $\mathrm{G}=O(1)$ and $\sin\alpha\approx\alpha=\epsilon\tilde{\alpha}=O(\epsilon)$;

(ii) $\mathrm{G}=\epsilon\tilde{\mathrm{G}}=O(\epsilon)$ and $\sin\alpha=O(1)$.

If we introduce a slow time variable $\tau=t/\epsilon$ in case (i), Eq. (50) can be approximated by an equation without convective terms (i.e., without Benney-type terms) but still with a hydrostatic term

$$h_\tau = -G\tilde{\alpha}[\partial_x F_1(h)] - \left[-GF_3(h)h_x + \frac{\mathrm{Ma}^\star\mathrm{Bi}^\star}{(1+\mathrm{Bi}^\star h)^2}F_4(h)h_x + F_3(h)\frac{1}{\mathrm{Bo}^\star}h_{xxx}\right]_x. \tag{55}$$

We have used $G\cos\alpha\approx G+O(\epsilon^2)$. This equation is asymptotically correct since it does not contain the expansion parameter ϵ anymore. Again, the limit $\mathrm{Da}\to 0$ of Eq. (55) leads to an equation describing a thin liquid film flowing on a slightly inclined plane.[14,16,17] The other limit $\mathrm{Da}\to\infty$ gives the exact result, i.e., the same equation as for $\mathrm{Da}\to 0$ but with h replaced by $h+\delta$. This is due to the use of the Darcy–Brinkman equation in the porous layer, which is similar to the Stokes equation in the fluid film and also because Eq. (55) can be directly derived using the Stokes equation for the liquid layer. Case (ii) leads to an equation similar to Eq. (55) but without the hydrostatic term when $\tilde{\alpha}$ is replaced by $\sin\alpha$ and G by $\tilde{G}$. For $\alpha=0$ we have a horizontal layer problem without evaporation and disjoining pressure.[8,17]

C. Slip approximation

Looking at the polynomial functions F_i [Eq. (51)] we observe that all the constants r_i scale as a length to a given power (see Appendix B). For instance, r_1, r_3, r_9, and r_{12} are proportional to the dimensionless length

$$l = \sqrt{\mathrm{Da}}(E_+ - E_-)/A, \tag{56}$$

while r_2, r_4, r_{10}, and r_{13} scale as a length squared, all the remaining r_i being proportional to a higher power of a length. Furthermore, if l is assumed to be small it can be shown that the F_i are dominated by the two highest power terms in h while the other terms are $O(l^2)$ or smaller. Under these circumstances, Eq. (50) reduces to

$$h_t = -\Gamma\left(\frac{h^3}{3}+lh^2\right)_x - \epsilon\left[\Gamma^2\left(\frac{2}{15}h^6+\frac{4}{5}lh^5\right)h_x - \Gamma\cot\alpha\left(\frac{1}{3}h^3+lh^2\right)h_x + \frac{\mathrm{Ma\,Bi}}{(1+\mathrm{Bi}\,h)^2}\left(\frac{h^2}{2}+lh\right)h_x + \frac{1}{\mathrm{Bo}^\star}\left(\frac{1}{3}h^3+lh^2\right)h_{xxx}\right]_x, \tag{57}$$

which is similar to the highest order truncation of the evolution equation (C6) derived for a thin liquid film on a smooth solid substrate with a slip boundary condition (Appendix C). This confirms the usefulness of replacing, in certain circumstances, the porous layer by an effective slip condition where

the slip coefficient l_s would be defined by Eq. (56). For $\chi=0$, the corresponding dimensional slip length is obtained from the porous layer characteristics as $\sqrt{\kappa b}\tanh(\sqrt{b/\kappa}d)$. Therefore, when d becomes large $l_s \sim \sqrt{\kappa b}$ that is the expression that can be obtained using the slip boundary condition[20] where the dimensionless slip coefficient is taken as $\gamma=\sqrt{\mu_{\text{eff}}/\mu_f}$.[26,33]

IV. LINEAR STABILITY ANALYSIS

A. General case

To asses the linear stability of the base flow of a flat film of thickness $h(x)=1$, the solution of Eq. (50) is written as $h=1+\tilde{\epsilon}\exp(\beta t)\exp(ikx)$ and then Eq. (50) is linearized in $\tilde{\epsilon}$. This provides sufficient conditions for instability. If we introduce the notation

$$f_2=\frac{2}{15}+\sum_{i=3}^{8} r_i,$$

$$f_3=\frac{1}{3}+\sum_{i=9}^{11} r_i, \tag{58}$$

$$f_4=\frac{1}{2}+r_{12}+r_{13},$$

the dispersion relation takes the form

$$i\beta_i+\beta_r=-i\Gamma(1+r_1+r_2)k+\frac{\epsilon}{\text{Bo}^\star}k^2(k_c^2-k^2)f_3, \tag{59}$$

where the critical wavenumber, k_c, is given by

$$k_c^2=\frac{\text{Bo}^\star}{f_3}\left[\Gamma^2 f_2-\Gamma\cot\alpha f_3+\frac{\text{Ma}^\star\text{Bi}^\star}{(1+\text{Bi}^\star)^2}f_4\right]. \tag{60}$$

The band of unstable wavenumbers lies between $k=0$ and k_c. The small amplitude surface waves at k_c travel downwards with the velocity

$$c=-\frac{\beta_i}{k}=\Gamma(1+r_1+r_2) \tag{61}$$

corresponding to twice the fluid velocity $u(h)$ at the surface of the undisturbed flat film. The onset of instability does not depend on the value of the parameter $\text{Bo}^\star$ and it occurs at zero wavenumber $k=k_c=0$ corresponding to a type II_s instability in the classification of Ref. 47. Therefore, the critical values of the dimensionless numbers $\text{Ma}^\star$, Γ, and $\text{Bi}^\star$ obey the following relationship:

$$0=\left[\Gamma_c^2 f_2-\Gamma_c\cot\alpha f_3+\frac{\text{Ma}_c^\star\text{Bi}_c^\star}{(1+\text{Bi}_c^\star)^2}f_4\right], \tag{62}$$

provided $f_3\neq 0$. Let us introduce the new dimensionless number

$$M=\frac{\text{Ma}^\star\text{Bi}^\star}{(1+\text{Bi}^\star)^2} \tag{63}$$

and represent its critical value as a function of Γ for different values of Da and b (Fig. 2). For $0<M<M_s=(f_3\cot\alpha)^2/4f_2f_4$ and small Γ the film is thermally unstable but is stabilized at moderate Γ by the flow itself. The stable region ends at higher Γ where a *convective* instability sets in. For $M>M_s$ the two instability ranges merge and the flow is unstable whatever the value of Γ. The general qualitative picture for the flow on a solid substrate[19] is not changed by porosity. However, when Da increases, the stable Γ number range is significantly reduced. Similarly, although hardly pronounced, increasing the porosity also destabilizes the film flow [Fig. 2(b)] and this effect is found to be more important for larger values of δ and Da (not represented in Fig. 2).

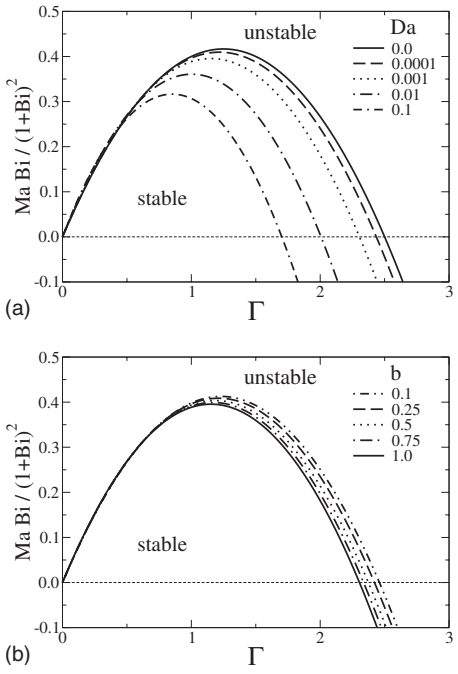

FIG. 2. Critical M [Eq. (63)] in dependence of the modified Galileo number for (a) different values of Da ($b=1.0$) and for (b) different values of b (Da=0.001). The other parameters are $\alpha=\pi/4$, $\chi=0$, and $\delta=0.1$.

The parabolic shape of the parameter range for linearly stable flat films allows for a characterization by the two parameters M_s and $\Gamma_c^\star$ at Ma=0. They are shown in dependence of Da for different values of the porosity b in Fig. 3 and on

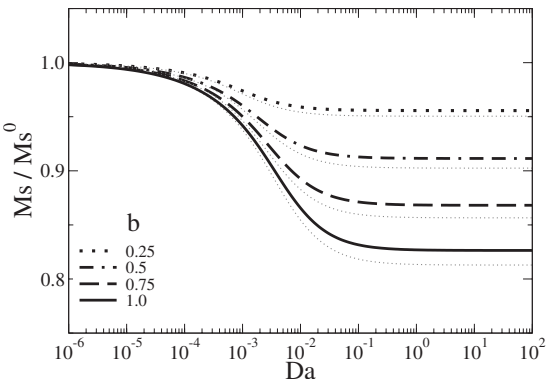

FIG. 3. Variation of the ratio M_s/M_s^0 ($M_s^0=M_s$ at Da=0) for different values of the Darcy number for fixed $b=1.0$, $\chi=0$, and $\delta=0.1$. Thin dotted lines give the corresponding results as obtained in the slip approximation [Eq. (57)].

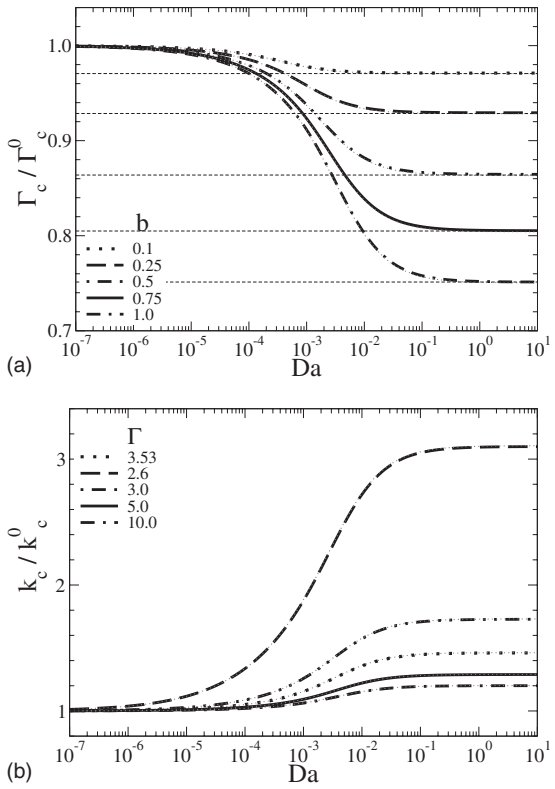

FIG. 4. Isothermal case (Ma=0). (a) Critical modified Galileo number for different porosities $b=0,\ldots,1$. (b) Critical wavenumber for selected supercritical modified Galileo numbers vs Da ($\delta=0.1$, ($b=1.0$), $\alpha=\pi/4$, and $\chi=0.0$). Both results are given as a ratio to the respective value for a thin film without the porous layer. The results are superposed with those obtained using the slip approximation [Eq. (57)] that are given as thin dotted lines.

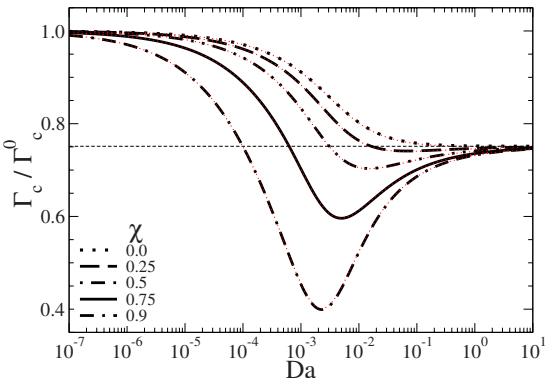

FIG. 5. (Color online) Influence of the stress jump coefficient χ on the critical modified Galileo number for different Darcy number ($\delta=0.1$, $\alpha=\pi/4$, and $b=1.0$. Thin dotted lines give the corresponding results as obtained in the slip approximation [Eq. (57)].

the top panel of Fig. 4, which is described in Sec. IV B. In Fig. 3, for small δ ($\delta=0.1$) the ratio M_s/M_s^0 ($M_s^0=M_s$ at Da=0) monotonically decreases with increasing Da and b. This is also well described by the slip approximation (thin lines).

B. Isothermal case

Under isothermal conditions (Ma=0) the critical modified Galileo number is given by

$$\Gamma_c = \cot\alpha \frac{f_3}{f_2}. \tag{64}$$

For the film of thickness unity on the solid substrate (Da $\to 0$) this criterion reduces to $\Gamma_c^0=\frac{5}{2}\cot\alpha$.[48,49] Figure 4 represents the change in the critical modified Galileo number with increasing Da for different values of porosity b. For several values of Γ the critical wavenumber is also plotted. The results clearly show that the porous layer and its permeability significantly influence the instability threshold and its length scale. Figures 4(a) and 4(b) show that for small thicknesses ($\delta=0.1$) the critical Γ (wavenumber) decreases (increases) monotonically with increasing Da for all parameter values. The change takes the form of a smooth step centered around Da$=10^{-4}-10^{-1}$. The plots show that for small δ, the slip approximation (Sec. III C) is very good since the curves obtained for Eq. (57) cannot be distinguished from the results obtained solving full problem (50). For a film on a solid substrate Γ_c scales as h_0^3. This together with the argument at the end of Sec. III A and the expression for r_3 in Eq. (54) points to the limit of $\Gamma_c/\Gamma_c^0=1/(1+b\delta)^3$ for Da$\to\infty$, where we have used $h_0=1$. These values agree well with the numerical results as indicated by the horizontal lines in Fig. 4(a).

Figure 5 shows the strong influence of the jump parameter χ for $\delta=0.1$. A nonmonotonic behavior is obtained. Indeed, first increasing Da leads to a strong decrease in Γ_c due to heterogeneities at the fluid-porous interface. When Da is large enough this effective slip effect progressively reduces and for large Da the ratio Γ_c/Γ_c^0 increases toward the value of the above given estimate $1/(1+b\delta)^3$, which is valid independently of χ (dotted horizontal line in Fig. 5). This behavior is also perfectly described by the slip approximation (the thin lines are superposed).

C. Low values of the modified Galileo number

For small Γ and case (i) (see Sec. III B) linearizing Eq. (55) yields the dispersion relation

$$i\beta_i + \beta_r = -iG\tilde{\alpha}(1+r_1+r_2)k + \frac{f_3}{\mathrm{Bo}^\star}k^2(k_c^2-k^2), \tag{65}$$

with

$$k_c^2 = \mathrm{Bo}^\star\left[\frac{\mathrm{Ma}^\star\,\mathrm{Bi}^\star}{(1+\mathrm{Bi}^\star)^2}\frac{f_4}{f_3} - G\right]. \tag{66}$$

The critical Marangoni number does not depend on the inclination α. It is given by

$$\mathrm{Ma}_c^\star = \frac{G(1+\mathrm{Bi}^\star)^2}{\mathrm{Bi}^\star}\frac{f_3}{f_4}. \tag{67}$$

In the limit of vanishing Da, e.g., for a smooth substrate at $z=0$, this reduces to $[2G(1+\mathrm{Bi}^\star)^2]/3\mathrm{Bi}^\star$ which corresponds to the known results for a horizontal[17,19] and slightly inclined[17] layer.

V. STATIONARY SOLUTIONS

To understand the behavior beyond the linear stage of exponentially growing harmonic surface modes one has to study the ongoing nonlinear dynamics. This can be done by numerically integrating Eq. (50) in time for a choice of parameter values. An alternative and very effective method determines analytically or numerically a single stationary solution (with respect to an appropriate comoving frame) and then uses path-following algorithms method to track this solution and its bifurcations in parameter space. This versatile method was recently applied to related thin film problems, e.g., to determine sitting,[50,51] sliding,[52] vibrating,[53] depinning,[54] and chemically driven running drops,[55] open two-layer films,[56] surface structures in reactive films,[57] and stratified states in demixing layers.[58] In the following we use continuation employing the numerical toolbox AUTO97 (Refs. 59–61) to determine spatially periodic steadily traveling solutions of Eq. (50), i.e., steady solutions of the equation in the frame moving with velocity c,

$$\Omega = \Gamma F_1 + \epsilon\left[\Gamma^2 F_2 h_x - \Gamma \cot \alpha F_3 h_x + \frac{\mathrm{Ma}^\star \mathrm{Bi}^\star}{(1+\mathrm{Bi}^\star h)^2} F_4 h_x + \frac{1}{\mathrm{Bo}^\star} F_3 h_{xxx}\right] - ch, \tag{68}$$

where the F_i are given by Eq. (51). The integration constant Ω represents the mean flow in the comoving frame. As starting solutions we take the small amplitude solutions obtained from the linearized problem. These harmonic surface waves have the period $L_c = 2\pi/k_c$ with k_c given by Eq. (60) and travel downward with the velocity given by Eq. (61).

Continuation in the period L and the velocity c yields a branch of stationary nonlinear solutions $h_0(x)$. These solve the nonlinear eigenvalue problem for the speed c specified by Eq. (68), subject to periodic boundary conditions with spatial period L. Fixing Ω the branch contains solutions with identical mean flow but varying mean thickness. Here, however, we are interested in solutions having identical mean film thickness. In this case Ω varies as additional continuation parameter necessary to maintain mass conservation $\int_0^L h_0 dx = 1$. Similar findings appear when the two cases are compared using a simpler Benney-type equation.[7]

To determine the stability of the stationary solutions $h_0(x)$ we use the Ansatz $h(x) = h_0(x) + \varepsilon h_1(x) e^{\beta t}$. Linearizing Eq. (50) in ε yields an eigenvalue problem for the growth rate β, and the associated eigenfunction $h_1(x)$. It is as well solved using continuation, starting from solutions obtained, as in Ref. 52. The employed procedure allows to solve for the stationary solutions [Eq. (50)] and the stability problem in parallel.[53,62]

The procedure may be started from a solution with period L_c or with period nL_c, where n is an integer. The resulting solution branches bifurcating from the uniform film will be called n-mode primary branches. We call the branches that bifurcate from these in secondary bifurcations as secondary solution branches. The $n > 1$ primary branches result directly from the $n = 1$ branch by multiplying the solution period by n. The corresponding solutions have an "internal symmetry" with respect to translations by L_c/n. Secondary bifurcations may either respect this discrete symmetry (these are saddle-node bifurcations that are already found for the $n = 1$ branch) or break it, creating a secondary branch of lower symmetry.[17]

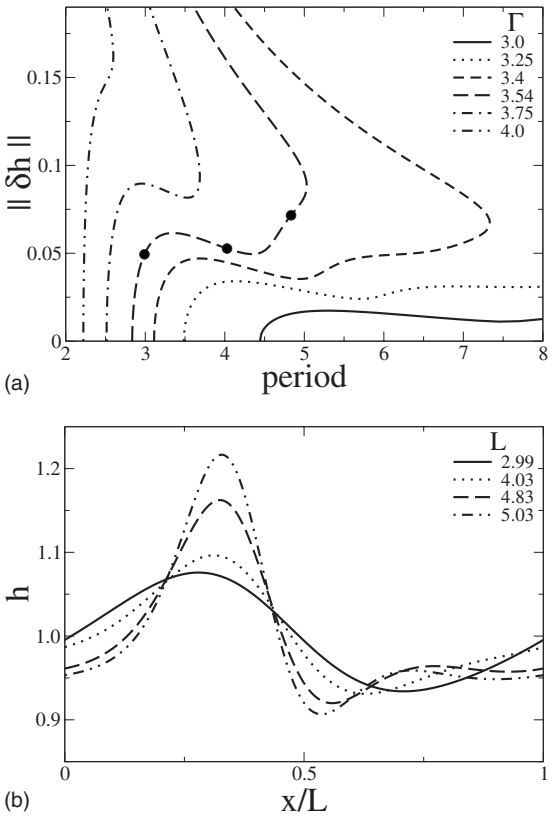

FIG. 6. Characterization of stationary solutions for a film on a solid substrate in the isothermal strongly inclined case, i.e., without porous layer (Da=0, Ma=0 and $\alpha = \pi/4$). (a) L_2 norm for the traveling wave solutions bifurcating from the flat film at L_c for different Γ. The full circles on the curves for $\Gamma = 3.54$ correspond to the solutions obtained in Ref. 19 by numerical integration in time. The corresponding profiles are plotted in (b).

Before embarking on the analysis of the most general case in Sec. III C to cross-check our methodology we discuss next some limiting cases that have been extensively studied in literature.

A. Strongly inclined isothermal wall

For the isothermal flow Fig. 6 shows for reference our results without porous layer. The individual stationary solutions are characterized by their L_2-norm $\|\delta h\| = [(1/L)\int_0^L (h(x) - h_0)^2 dx]^{1/2}$, where L is the period. For different Γ values, the families of stationary solutions are presented in Fig. 6(a) while Fig. 6(b) gives selected stationary film thickness profiles. The results for $\Gamma = 3.54$ correspond directly to time simulations performed in Ref. 19. Inspecting Fig. 6(a) the curve for $\Gamma = 3.54$ shows that stationary solutions exist in the range $L_c \approx 3 \leq L \leq 5$. This corresponds to the convergence of the time evolutions shown for $k = 2.1$, 1.56, and 1.3 shows these in the respective Figs. 5, 6, and 7 of Ref. 19. Figure 6(b) shows the profiles of these surface waves. The velocity of the waves increases with increasing Γ number or increasing period (not represented here). The

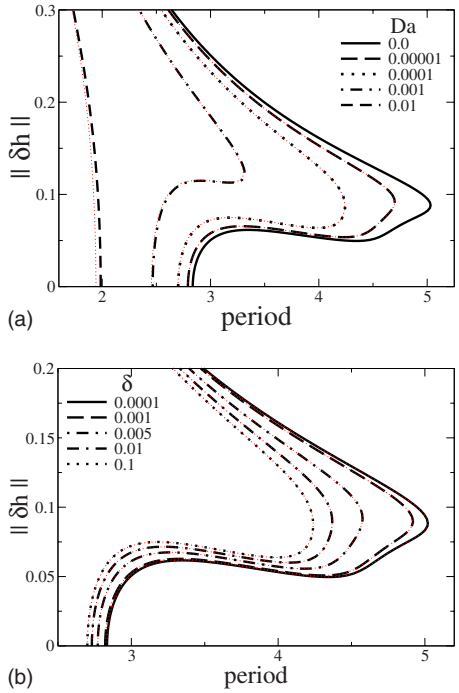

FIG. 7. (Color online) Families of stationary solutions for a film on a porous substrate in the isothermal strongly inclined case. (a) L_2 norm of the wave solutions for $\Gamma=3.54$, $\delta=1.0$, and different Da. (b) L_2 norm for $\Gamma=3.54$, Da=0.0001, and different δ. The other parameters are $b=1.0$, $\chi=0.0$, and $\alpha=\pi/4$. Thin dotted lines give the corresponding results as obtained in the slip approximation [Eq. (57)].

saddle-node bifurcation at $L_s\approx 5$ limits the wavenumber range where the nonlinear evolution saturates. This explains why Fig. 8 (at $k=1.11$) and Fig. 9 (at $k=0.7$) in Ref. 19 show no equilibration of the flow. The locus of the saddle-node strongly depends on Γ [Fig. 6(a)]. For Γ close to onset the solution branch continues toward diverging period, as shown for $\Gamma=3$. Increasing Γ the saddle-node appears at infinity and moves rapidly to smaller periods. When it reaches L_c the primary bifurcation becomes subcritical. This saddle node is a property of the thin film equation with a Benney-type term and is not found in the full hydrodynamic description.[5–7] The Benney-type thin film equation gives only acceptable results for structures smaller than L_s.

Let us now consider the isothermal film flow on the porous wall and calculate solution branches for several values of the modified Galileo number and for different properties of the porous medium. The influence of the Darcy number is qualitatively very similar for different Γ and δ. Figure 7 gives a typical example using $\Gamma=3.54$. With increasing Da, the critical wavelength decreases and the period range where stable stationary wave solutions exist becomes smaller. The L_2 norm [Fig. 7(a)], amplitude, and velocity (not shown here) increase with increasing Da for L in the saturation range. Comparison with Fig. 6 indicates that the overall influence of increasing Da is very much like that for increasing Γ.

The influence of the thickness of the porous layer δ at fixed Da is plotted in Fig. 7(b). Interestingly, thickness changes in a very thin layer between $\delta=10^{-4}$ and 0.1 have a noticeable influence shifting L_c and L_s to smaller values and slightly increasing the L_2 norm, a behavior already seen for increasing Da. In contrast a further increase seems to have nearly no impact, the influence of the porous layer "saturates." The thickness of the layer where this happens increases with Da.

Figure 7 also shows with thin lines the features of the branches calculated in the slip approximation using the stationary equation derived from Eq. (C6) with the slip length l_s from Eq. (56). Surprisingly, the slip approximation gives quite an accurate result also for the nonlinear behavior. It leads, however, to not so good results for large Da or δ, which corresponds to a parameter range of not much interest because there, the branches of stationary solutions always bifurcate subcritically and do not represent physical solutions.[7]

The conclusion of the present section is that although a porous substrate has a strong influence on both the linear stability and the nonlinear behavior it can for small and moderate Darcy number and thickness of the porous layer be mimicked to perfection by replacing the porous layer by an *ad hoc* appropriate slip condition at a smooth substrate.

B. Slightly inclined heated substrate

Next, we study the stationary solutions for a heated, slightly inclined plate as described by Eq. (55). For a solid substrate it is known that increasing the inclination angle from zero to a finite but still small value a transition occurs from traveling large amplitude structures (sliding drops) to small amplitude surface waves, representing a transition from Cahn–Hilliard-type dynamics to Kuramoto–Sivashinsky-type dynamics.[17] In contrast to the isothermal case with large inclination studied in Sec. V A here all solutions including the ones of large amplitude represent physical solutions that can as well be obtained using Stokes equations (see Ref. 63 for $\alpha=0$). The transition from drops to surface waves is a result of the competition of vertical Marangoni driving (favoring drops) and lateral gravitational driving (favoring surface waves). In our case, we find that a porous substrate underlying the liquid film shifts this transition toward smaller inclinations. Figure 8 summarizes the influence of the Darcy number and the thickness of the porous layer δ on the $n=1$ solution branch for a small inclination angle ($\alpha=0.2$) and for Ma=3.5.

The shift of the transition region (as compared to the case with Da=0) is significant [Figs. 8(a) and 8(b)]. There for small Da each branch has three sub-branches: one of small amplitude solutions (surface waves) another one of large amplitude solutions (sliding drops or holes) and an unstable intermediate branch. With increasing Da the surface wave part of the branch extends toward larger periods. The amplitude of the waves decreases with increasing Da. The large amplitude part of the branch for $\delta=0.1$ is affected little by changes in Da [Fig. 8(a)]. However, for $\delta=3.0$ the lower limiting period of the large amplitude part of the branch significantly increases, and the existence range of large amplitude structures becomes smaller. This leads eventually to the disappearance of the large amplitude solutions [Fig. 8(b)]. A similar transition from droplike to surface wave solutions is found when increasing the inclination for fixed Da. Note

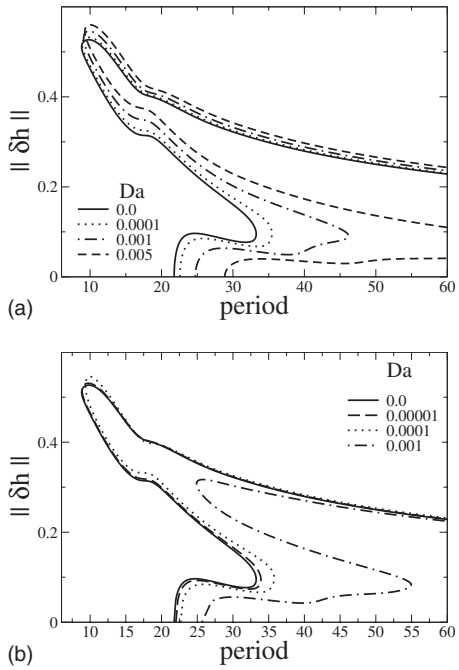

FIG. 8. Families of stationary solutions for a film on a porous substrate in the small inclination regime for different Da. Shown is the L_2 norm for (a) $\delta=0.1$, $\alpha=0.2$, and (b) $\delta=3.0$, $\alpha=0.2$. The remaining parameters are Ma $=3.5$, $b=1.0$, $G=1.0$, Bi$=0.5$, Bo$=0.5$, and $\chi=0.0$.

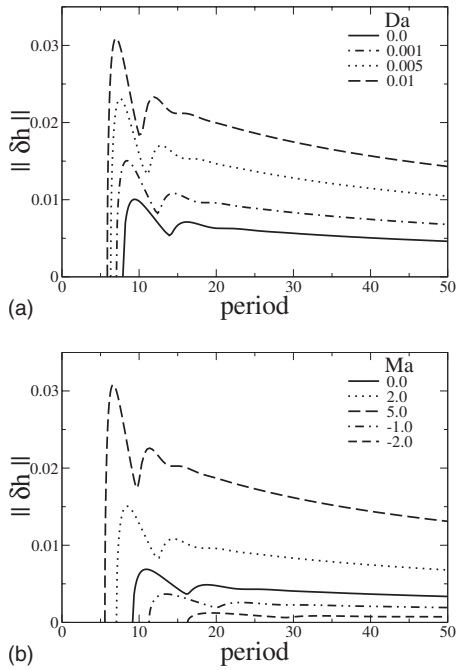

FIG. 10. Families ($n=1$ branch) of stationary traveling surface waves for a strongly inclined heated plate for (a) fixed Ma$=2.0$ and different Da, (b) fixed Da$=0.001$, and different Ma. Shown is the L_2 norm. The remaining parameters are $\delta=0.1$, $b=1.0$, $\Gamma=3.0$, $\alpha=\pi/4$, Bo$=0.5$, Bi$=0.5$, and $\chi=0.0$.

finally that in correspondence with the linear stability analysis the branching point from the flat film state (at the critical period) shifts toward larger periods with increasing Da. This is due to the larger stabilizing effect of the lateral flow for larger effective film thickness, i.e., for larger Da.

We analyze the transition further by following in parameter space the loci of the main saddle-node bifurcations of the branches shown in Fig. 8. Figure 9 shows these loci together with those of the primary bifurcation [at L_c given by Eq. (66)] as a function of Da for $\delta=0.1$ and fixed inclination $\alpha=0.2$. It also indicates the resulting existence ranges of droplike solutions (left-hatched) and surface waves (right-hatched). The region where both may exist is cross hatched. For the chosen angle two saddle-node bifurcations are present even at very small Da. We emphasize that in contrast

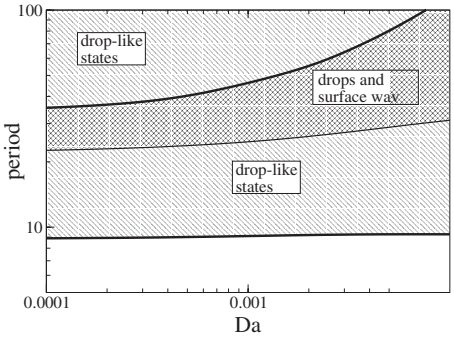

FIG. 9. Loci of the primary bifurcation (thin lines) and main saddle-node bifurcations (heavy lines) of the $n=1$ branch of stationary solutions and existence ranges for droplike states and surface waves in the (Da, period) plane for $\alpha=0.2$ and thicknesses of the porous layer $\delta=0.1$. The remaining parameters are Ma$=3.5$, $b=1.0$, $G=1.0$, Bi$=0.5$, Bo$=0.5$, and $\chi=0.0$.

to the strongly inclined isothermal case (Sec. V A) both indicate qualitative changes in the behavior of the physical system. The first saddle-node bifurcation is located at a $L_{sn1}>L_c$ and gives the maximal period of surface waves. The second one is for small Da located at a $L_{sn2}<L_c$. In the range $L_{sn2}<L<\infty$ droplike states exist. For $\delta=0.1$ the locus L_{sn2} of the second saddle-node bifurcation remains essentially unchanged. This implies that for larger Da there is a large period range where droplike solutions and surface waves may coexist. The linearly unstable nucleation solution situated in Fig. 8 in between the droplike and the surface wave solutions exist between the two heavy lines in Fig. 9.

The droplike and the surface wave solutions are linearly stable to nonoscillatory disturbances that have the same period as the base solution. However, they may be unstable to (i) oscillatory modes or (ii) nonoscillatory disturbances whose period is a multiple of the period as the base solution (coarsening modes). We find that the porous substrate does not change qualitatively the stability properties relative to a heated film on an inclined substrate without porous layer.[17]

C. The general case

Let us now discuss a few results for the case of a strongly inclined heated plate. Thereby we focus on stationary traveling surface waves by choosing parameter values for which the solution families show no saddle-node bifurcation. This ensures that the studied solutions are of experimental relevance.[7]

Equation (68) is solved using continuation techniques as before. In Fig. 10 we present characteristics of the surface waves of the $n=1$ primary branch for varying Darcy and Marangoni numbers. With increasing Da the critical wave-

length decreases whereas the amplitude and velocity of the waves increase [Fig. 10(a)]. The decrease in the critical wavelength corresponds to results of the linear stability results. It is due to an increase in effective film thickness with increasing Da, i.e., to an increase in destabilizing inertia. Note that this contrasts the stabilizing influence of flow for a slightly inclined plate (see Sec. V B).

Similar results are presented in Fig. 10(b) for increasing Ma. There it is also shown that cooling from below, hence Ma becoming negative, leads to a "stabilization" of the traveling waves, i.e., decreasing Ma below zero the amplitude and velocity of the waves decrease. This can be expected from the discussion in Sec. IV.

VI. CONCLUSIONS

In the present work we have studied the stability and evolution of a thin liquid film with a free surface flowing down an inclined heated solid porous wall. Using lubrication approximation, an evolution equation for the film thickness profile was derived whose limiting cases in terms of permeability, porosity, inclination, or Galileo numbers have been examined. The film thickness equation incorporates convective (Benney) terms allowing to study the interplay of convective and thermocapillary instabilities thus extending the work done for a thin film on a smooth substrate.[19] As with all Benney-type equations our equation has, however, for stronger flow only a limited validity range since it leads to blow-up of solutions in finite time corresponding to an unphysical saddle-node bifurcation in our analysis of stationary solutions in the strongly inclined case. This shortcoming does not exist when discussing the limit of a slightly inclined heated substrate or creeping flow in a very thin film. In such cases, the convective instability mechanism is absent and hence the study has focused on the thermocapillary instability. For completeness and to compare with the more complete above equation we have also derived the corresponding equations for the slipping liquid film on both a strongly and a slightly inclined smooth solid substrate. However, we have neglected the thermocapillary short-wave instability[10] thus restricting the practical application of our analysis to thin films.

Our analysis of the evolution equation indicates that the substrate porosity has in general a *destabilizing* influence upon the liquid film flow. This has been shown for a flat film (a) on a strongly inclined isothermal substrate, (b) on a slightly inclined or horizontal heated substrate, and (c) for the general case of a strongly inclined heated substrate. As expected, heterogeneities at the fluid-porous interface play a destabilizing role at moderate values of the Darcy number. They also decrease the range where stable surface waves can be found in the highly inclined isothermal case. Furthermore, with a slightly inclined substrate, increasing the Darcy number or the layer thickness can turn subcritical primary bifurcations into supercritical ones. It thereby favors the appearance of small amplitude surface waves. Note, however, that the surface waves do not directly replace the large amplitude droplike states but can coexist with them in a wide range of parameter values. In this way the porous substrate shifts the transition from Cahn–Hilliard-type dynamics to Kuramoto–Sivashinsky-type dynamics[17] toward smaller inclination angles.

A deeper understanding of the effect of a porous substrate has emerged from a comparison of the full models and the reduced slip models. It appears that for thin enough porous layers both approaches agree very well if the dimensional slip length is chosen as $l_s=\sqrt{\kappa b}\tanh(\sqrt{b/\kappa}d)$. For a thick porous substrate the slip length approaches the limiting value $\sqrt{\kappa b}$ that can also be obtained from the slip boundary condition introduced by Beavers and Joseph.[20] The great advantage of such a relation between an effective slip length and the thickness and properties of the porous substrate rests on the fact that it is possible to describe the roughness of a surface as a saturated porous layer with well defined characteristics. This implies that one can model a thin film flow on a rough substrate in a quantitatively correct way by first deriving effective parameters for the porous layer and then using them to determine an effective slip length. However, this approximation is not valid for large values of the Darcy number and thick porous layers. Yet it is a very good approximation for thick porous layers for low values of the Darcy number.

ACKNOWLEDGMENTS

U.T. acknowledges support through the EU RTN "Unifying principles in non-equilibrium pattern formation" (Contract No. MRTN-CT-2004–005728). This research was also supported in part by Grant No. MEC-VEVES-FIS2006-01305 of the Spanish Ministerio de Educacion y Ciencia.

APPENDIX A: $O(1)$ AND $O(\epsilon)$ PROBLEMS

Introducing Eq. (37) into the dimensionless equations (19)–(22) and boundary conditions (26)–(29) leads to problems of orders $O(1)$ and $O(\epsilon)$ in both fluid and porous regions. The system of order $O(1)$ in the fluid is given by

$$0 = u_{0zz} + G\sin\alpha, \tag{A1}$$

$$0 = p_{0z} + G\cos\alpha, \tag{A2}$$

$$0 = T_{0zz}, \tag{A3}$$

$$0 = u_{0x} + w_{0z}, \tag{A4}$$

while the equivalent in the porous medium takes the form

$$0 = \frac{1}{b}\tilde{u}_{0zz} - \frac{1}{\mathrm{Da}}\tilde{u}_0 + G\sin\alpha, \tag{A5}$$

$$0 = \tilde{p}_{0z} + G\cos\alpha, \tag{A6}$$

$$0 = \tilde{T}_{0zz}, \tag{A7}$$

$$0 = \tilde{u}_{0x} + \tilde{w}_{0z}. \tag{A8}$$

The associated boundary conditions are

$$u_{0z} = 0 \quad \text{at} \quad z = h, \tag{A9}$$

$$-p_0 = \frac{1}{\mathrm{Bo}^*} h_{xx} \quad \text{at} \quad z = h, \tag{A10}$$

$$\tilde{\mathbf{u}}_0 = \mathbf{u}_0 \quad \text{at} \quad z = 0, \tag{A11}$$

$$\tilde{p}_0 = p_0 \quad \text{at} \quad z = 0, \tag{A12}$$

$$\frac{1}{b}\tilde{u}_{0z} - u_{0z} = \frac{\chi}{\sqrt{\mathrm{Da}}}\tilde{u}_0 \quad \text{at} \quad z = 0, \tag{A13}$$

$$\tilde{\mathbf{u}}_0 = 0 \quad \text{at} \quad z = -\delta, \tag{A14}$$

$$0 = T_{0z} + \mathrm{Bi}\, T_0 \quad \text{at} \quad z = h, \tag{A15}$$

$$T_0 = 1 \quad \text{at} \quad z = -\delta, \tag{A16}$$

$$T_0 = \tilde{T}_0 \quad \text{at} \quad z = 0, \tag{A17}$$

$$T_{0z} = \Lambda_{\mathrm{eff}} \tilde{T}_{0z} \quad \text{at} \quad z = 0, \tag{A18}$$

$$w_0 - h_\tau - u_0 h_x = 0 \quad \text{at} \quad z = h. \tag{A19}$$

The relevant equations to order $O(\epsilon)$ in the liquid can be written as

$$(u_{0\tau} + u_0 u_{0x} + w_0 u_{0z}) = -p_{0x} + u_{1zz}, \tag{A20}$$

$$0 = u_{1x} + w_{1z}, \tag{A21}$$

while in the porous medium they take the form

$$\frac{1}{b}\tilde{u}_{0\tau} = -\tilde{p}_{0x} + \frac{1}{b}\tilde{u}_{1zz} - \frac{1}{\mathrm{Da}}\tilde{u}_1, \tag{A22}$$

$$0 = \tilde{u}_{1x} + \tilde{w}_{1z}. \tag{A23}$$

Finally, the boundary conditions for order $O(\epsilon)$ are given by

$$u_{1z} = -\mathrm{Ma}(T_{0x} + h_x T_{0z}) \quad \text{at} \quad z = h, \tag{A24}$$

$$\tilde{\mathbf{u}}_1 = \mathbf{u}_1 \quad \text{at} \quad z = 0, \tag{A25}$$

$$\frac{1}{b}\tilde{u}_{1z} - u_{1z} = \frac{\chi}{\sqrt{\mathrm{Da}}}\tilde{u}_1 \quad \text{at} \quad z = 0, \tag{A26}$$

$$\tilde{\mathbf{u}}_1 = 0 \quad \text{at} \quad z = -\delta, \tag{A27}$$

$$w_1 - h_{\tau_1} - u_1 h_x = 0 \quad \text{at} \quad z = h. \tag{A28}$$

Let us remark that the $O(\epsilon)$ equations involving T_1 and p_1 are not given since they are not necessary for the derivation of the film thickness equation to $O(\epsilon)$.

APPENDIX B: CALCULATION OF CONSTANTS

Equation (38) with boundary condition (A9) yields

$$C_0 = G \sin \alpha h \tag{B1}$$

and Eq. (39) with the normal stress condition (A10) determines

$$C_2 = G \cos \alpha h - \frac{1}{\mathrm{Bo}^\star} h_{xx}. \tag{B2}$$

Combining Eqs. (38) and (40) with the boundary conditions (A11), (A13), and (A14) gives

$$C_3 = -\frac{G \sin \alpha\, \mathrm{Da}\, B_- + E_-(C_0\sqrt{\mathrm{Da}} + \chi G \sin \alpha\, \mathrm{Da})}{A}, \tag{B3}$$

$$C_4 = -\frac{1}{E_-}[G \sin \alpha\, \mathrm{Da} + C_3 E_+], \tag{B4}$$

and

$$C_1 = G \sin \alpha\, \mathrm{Da} + C_3 + C_4 \tag{B5}$$

where

$$E_+ = e^{\sqrt{b/\mathrm{Da}}\,\delta} \quad \text{and} \quad E_- = e^{-\sqrt{b/\mathrm{Da}}\,\delta},$$

$$B_+ = \frac{1}{\sqrt{b}} + \chi \quad \text{and} \quad B_- = \frac{1}{\sqrt{b}} - \chi, \tag{B6}$$

$$A = E_+ B_- + E_- B_+.$$

The coefficients for the temperature field equation (41) are given by the thermal boundary conditions (A15) and (A16)

$$C_5 = -\frac{\mathrm{Bi}}{1 + \mathrm{Bi}(h + \delta/\Lambda_{\mathrm{eff}})}, \tag{B7}$$

$$C_6 = 1 + \frac{\mathrm{Bi}\,\delta}{\Lambda_{\mathrm{eff}}[1 + \mathrm{Bi}(h + \delta/\Lambda_{\mathrm{eff}})]}. \tag{B8}$$

Equation (44) and the no-penetration condition (A14) yield

$$C_8 = (C_8^i)_x = \sqrt{\mathrm{Da}/b}(C_4 E_- - C_3 E_+)_x. \tag{B9}$$

Then Eqs. (43) and (A11) give

$$C_7 = (C_7^i)_x = [\sqrt{\mathrm{Da}/b}(C_3 - C_4) + C_8^i]_x. \tag{B10}$$

The integration constants for the solutions of the $O(\epsilon)$ problem are obtained as follows. Equation (45) and condition (A24) provide

$$C_9 = -\frac{1}{6}(C_0 C_{0x} + G\sin\alpha C_{1x})h^3 - \frac{1}{2}(C_{0\tau} + C_{0x}C_1 - G\sin\alpha C_7)h^2 - (C_{2x} + C_{1\tau} + C_1 C_{1x} + C_0 C_7)h + \mathrm{Ma}\frac{\mathrm{Bi}\, h_x}{[1+\mathrm{Bi}(h+\delta/\Lambda_{\mathrm{eff}})]^2}. \tag{B11}$$

Then Eqs. (45) and (46) and the boundary conditions (A25)–(A27) give

$$C_{11} = -\frac{1}{A}\left[E_-\sqrt{\mathrm{Da}}\, C_9 - (B_- + \chi E_-)\mathrm{Da}\, C_{2x} + \frac{1}{2b}\left(\sqrt{b\mathrm{Da}}\,\delta B_- E_+ + \frac{\mathrm{Da}}{\sqrt{b}}E_-\right)C_{3\tau} - \frac{1}{2b}\left(\sqrt{b\mathrm{Da}}\,\delta B_- E_- + \frac{\mathrm{Da}}{\sqrt{b}}E_-\right)C_{4\tau}\right], \tag{B12}$$

$$C_{12} = \frac{1}{B_-}\left(\frac{1}{2b}\frac{\mathrm{Da}}{\sqrt{b}}(C_{3\tau} - C_{4\tau}) + \sqrt{\mathrm{Da}}\, C_9 - \chi\mathrm{Da}\, C_{2x} + B_+ C_{11}\right), \tag{B13}$$

$$C_{10} = -\mathrm{Da}\, C_{2x} + C_{11} + C_{12}. \tag{B14}$$

Equation (48) and the no-penetration condition (A27) yield

$$C_{14} = (C_{14}^i)_x = \left[\mathrm{Da}\,\delta C_{2x} + \frac{1}{2}\sqrt{\frac{\mathrm{Da}}{b}}\left(\frac{\mathrm{Da}}{b}C_{3\tau} - 2C_{11} - \sqrt{\frac{\mathrm{Da}}{b}}C_{3\tau}\delta\right)E_+ - \frac{1}{2}\sqrt{\frac{\mathrm{Da}}{b}}\left(\frac{\mathrm{Da}}{b}C_{4\tau} - 2C_{12} + \sqrt{\frac{\mathrm{Da}}{b}}C_{4\tau}\delta\right)E_-\right]_x, \tag{B15}$$

while C_{13} is given by Eq. (47) and condition (A25),

$$C_{13} = (C_{13}^i)_x = \left[-\frac{1}{2}\sqrt{\frac{\mathrm{Da}}{b}}\left(\frac{\mathrm{Da}}{b}C_{3\tau} - 2C_{11}\right) + \frac{1}{2}\sqrt{\frac{\mathrm{Da}}{b}}\left(\frac{\mathrm{Da}}{b}C_{4\tau} - 2C_{12}\right) + C_{14}^i\right]_x. \tag{B16}$$

Finally, the film thickness equation in terms of the above constants can be written as

$$h_t = -\left[\frac{C_0}{2}h^2 + C_1 h - \frac{G\sin\alpha}{6}h^3 - C_7^i\right]_x - \epsilon\left[\frac{1}{120}(C_0 C_{0x} + G\sin\alpha C_{1x})h^5 + \frac{1}{24}(C_{0\tau} + C_{0x}C_1 - G\sin\alpha C_7)h^4 + \frac{1}{6}(C_{2x} + C_{1\tau} + C_1 C_{1x} + C_0 C_7)h^3 + \frac{1}{2}C_9 h^2 + C_{10}h - C_{13}^i\right]_x. \tag{B17}$$

Then, the expressions for C_i, $i=0,\ldots,14$ are introduced in Eq. (B17) and after some rather tedious algebra the film evolution equation (50) is obtained as given in the main body of the paper. The constants r_i, depending on the properties of the porous layer, are

$$r_1 = 2\frac{\sqrt{\mathrm{Da}}}{A}(E_+ - E_-), \tag{B18}$$

$$r_2 = \frac{2\mathrm{Da}}{A\sqrt{b}}(E_+ + E_- - 2), \tag{B19}$$

$$r_3 = \frac{4}{5}\frac{\sqrt{\mathrm{Da}}}{A}(E_+ - E_-), \tag{B20}$$

$$r_4 = \frac{5}{3}\frac{\mathrm{Da}}{A^2}\left[(E_+ - E_-)^2 + \frac{2}{5}\frac{A}{\sqrt{b}}(E_+ + E_- - 2)\right], \tag{B21}$$

$$r_5 = \frac{\mathrm{Da}^{3/2}}{A^2}\left[\frac{8}{3\sqrt{b}}(E_+ - E_-)(E_+ + E_- - 2) + \frac{1}{A}(E_+ - E_-)^3 + \frac{1}{2b\sqrt{b}}(E_+^2 - E_-^2)\right] - \frac{2\mathrm{Da}}{A^2 b}\delta, \tag{B22}$$

$$r_6 = \frac{\mathrm{Da}^2}{2Ab^{3/2}}[E_+ + E_- - 2] + \frac{\mathrm{Da}^2}{2A^2b^2}[2 + (-2+E_-)E_- + (-2+E_+)E_+ + 2\{6 + (-4+E_-)E_- + (-4+E_+)E_+\}\sqrt{b}] + \frac{\mathrm{Da}^2}{2A^3b^2}[\{-2(E_- + E_+) + 2(E_-^3 + E_+^3)\}\sqrt{b} + 4\{4 + E_-[-1 + (-2+E_-)E_-] + E_+[-1 + (-2+E_+)E_+]\}b^{3/2}] + \frac{\mathrm{Da}^{3/2}\,\delta}{A^2 b}\left[\chi(E_+ + E_- - 2) - \frac{1}{\sqrt{b}}(E_+ - E_-) - \frac{4}{A}(E_+ - E_-)\right], \tag{B23}$$

$$r_7 = \frac{\mathrm{Da}^{5/2}}{A^3 b^2}[(E_+ + E_- - 2)b + (E_+ + E_-) + (E_- + E_+ + \sqrt{b}A)] \times (E_+ - E_-)(E_+ + E_- - 2) + \frac{2\mathrm{Da}^2\ \delta}{A^3 b}\left[\left(\chi(E_+ + E_- - 2) - \frac{1}{\sqrt{b}}(E_+ - E_-)(E_+ - E_-) - \frac{2}{\sqrt{b}}(E_+ + E_- - 2)\right)\right], \tag{B24}$$

$$r_8 = \frac{\mathrm{Da}^{5/2}}{A^3 b\sqrt{b}}\left\{2\delta\left[\chi(E_+ + E_- - 2) - \frac{1}{\sqrt{b}}(E_+ - E_-)\right] + \frac{\mathrm{Da}^{1/2}}{b}(E_+ + E_- - 2)(E_- + E_+ + \sqrt{b}A)\right\}(E_+ + E_- - 2), \tag{B25}$$

$$r_9 = \frac{\sqrt{\mathrm{Da}}}{A}(E_+ - E_-), \tag{B26}$$

$$r_{10} = \frac{2\mathrm{Da}}{A\sqrt{b}}(E_+ + E_- - 2), \tag{B27}$$

$$r_{11} = \frac{\mathrm{Da}^{3/2}}{Ab}[2\chi\sqrt{b}(E_+ + E_- - 2) - (E_+ - E_-)] + \mathrm{Da}\ \delta, \tag{B28}$$

$$r_{12} = \frac{\sqrt{\mathrm{Da}}}{A}(E_+ - E_-), \tag{B29}$$

$$r_{13} = \frac{\mathrm{Da}}{A\sqrt{b}}(E_+ + E_- - 2). \tag{B30}$$

APPENDIX C: LIQUID FILM ON A SOLID SUBSTRATE WITH A SLIP BOUNDARY CONDITION

In this section the film thickness evolution equation is derived assuming that the porous layer can be replaced by a slip condition at the solid substrate. In that "slip" case, the dimensionless equations reduce to Eqs. (18) and (19) with boundary conditions (26)–(29) while conditions (32)–(36) are replaced by

$$w = 0 \quad \text{at} \quad z = 0, \tag{C1}$$

$$u = l_s u_z \quad \text{at} \quad z = 0, \tag{C2}$$

$$T = 1 \quad \text{at} \quad z = 0, \tag{C3}$$

where l_s is the dimensionless slip length.[64] The velocity field is then given by Eqs. (38), (43), (45), and (47) where C_0, C_2, and C_9 are the same as before, $C_7 = C_{13} = 0$ and

$$C_1 = l_s C_0, \tag{C4}$$

$$C_{10} = l_s C_9. \tag{C5}$$

After some algebra the film thickness evolution equation with a slip boundary condition on the solid substrate takes the form

$$h_t = -\Gamma\left(\frac{1}{3}h^3 + l_s h^2\right)_x - \epsilon\left[\Gamma^2\left(\frac{2}{15}h^6 + \frac{4}{5}l_s h^5 + \frac{5}{3}l_s^2 h^4 + l_s^3 h^3\right)h_x - \Gamma\cot\alpha\left(\frac{1}{3}h^3 + l_s h^2\right)h_x + \mathrm{Ma}\left(\frac{1}{2}h^2 + l_s h\right)\frac{\mathrm{Bi}\ h_x}{(1 + \mathrm{Bi}\ h)^2} + \left(\frac{1}{3}h^3 + l_s\ h^2\right)\frac{1}{\mathrm{Bo}^\star}h_{xxx}\right]_x. \tag{C6}$$

Comparing Eqs. (C6) and (50) taking into account the definitions of the r_i shows that the highest order slip terms in Eq. (C6) are of similar form as the leading order corrections that derive from the porous layer in Eq. (50). The respective leading terms are identical when identifying l_s in Eq. (C6) with $l = \sqrt{\mathrm{Da}}(E_+ - E_-)/A$ in Eq. (50).

[1] H.-C. Chang, "Wave evolution on a falling film," Annu. Rev. Fluid Mech. **26**, 103 (1994).
[2] A. Oron, S. H. Davis, and S. G. Bankoff, "Long-scale evolution of thin liquid films," Rev. Mod. Phys. **69**, 931 (1997).
[3] D. J. Benney, "Long waves on liquid films," J. Math. Phys. (Cambridge, Mass.) **45**, 150 (1966).
[4] P. Rosenau, A. Oron, and J. Hyman, "Bounded and unbounded patterns of the Benney equation," Phys. Fluids A **4**, 1102 (1992).
[5] T. R. Salamon, R. C. Armstrong, and R. A. Brown, "Traveling waves on vertical films: Numerical analysis using the finite element method," Phys. Fluids **6**, 2202 (1994).
[6] A. Oron and O. Gottlieb, "Nonlinear dynamics of temporally excited falling liquid films," Phys. Fluids **14**, 2622 (2002).
[7] B. Scheid, C. Ruyer-Quil, U. Thiele, O. A. Kabov, J. C. Legros, and P. Colinet, "Validity domain of the Benney equation including Marangoni effect for closed and open flows," J. Fluid Mech. **527**, 303 (2005).
[8] J. P. Burelbach, S. G. Bankoff, and S. H. Davis, "Nonlinear stability of evaporating/condensing liquid films," J. Fluid Mech. **195**, 463 (1988).
[9] J. P. Burelbach, S. G. Bankoff, and S. H. Davis, "Steady thermocapillary flows of thin liquid layers. II. Experiment," Phys. Fluids A **2**, 322 (1990).
[10] A. A. Golovin, A. A. Nepomnyashchy, and L. M. Pismen, "Interaction between short-scale Marangoni convection and long-scale deformational instability," Phys. Fluids **6**, 34 (1994).
[11] S. J. VanHook, M. F. Schatz, W. D. McCormick, J. B. Swift, and H. L. Swinney, "Long-wavelength instability in surface-tension-driven Bénard convection," Phys. Rev. Lett. **75**, 4397 (1995).
[12] S. J. VanHook, M. F. Schatz, J. B. Swift, W. D. McCormick, and H. L. Swinney, "Long-wavelength surface-tension-driven Bénard convection: Experiment and theory," J. Fluid Mech. **345**, 45 (1997).
[13] P. Colinet, J. C. Legros, and M. G. Velarde, *Surface-Tension-Driven Instabilities* (Wiley-VCH, Berlin, 2001).
[14] A. Oron and P. Rosenau, "Formation of patterns induced by thermocapillarity and gravity," J. Phys. II **2**, 131 (1992).
[15] A. Oron and S. G. Bankoff, "Dynamics of a condensing liquid film under conjoining/disjoining pressures," Phys. Fluids **13**, 1107 (2001).
[16] M. Bestehorn, A. Pototsky, and U. Thiele, "3D large scale Marangoni convection in liquid films," Eur. Phys. J. B **33**, 457 (2003).
[17] U. Thiele and E. Knobloch, "Thin liquid films on a slightly inclined heated plate," Physica D **190**, 213 (2004).
[18] V. M. Starov, M. G. Velarde, and C. J. Radke, *Wetting and Spreading Dynamics* (Taylor & Francis, Boca Raton, FL, 2007).

[19]S. W. Joo, S. H. Davis, and S. G. Bankoff, "Long-wave instabilities of heated falling films: Two-dimensional theory of uniform layers," J. Fluid Mech. **230**, 117 (1991).
[20]G. S. Beavers and D. D. Joseph, "Boundary conditions at a naturally permeable wall," J. Fluid Mech. **30**, 197 (1967).
[21]P. G. Saffman, "On the boundary condition at the surface of a porous medium," Stud. Appl. Math. **50**, 93 (1971).
[22]G. S. Beavers, E. M. Sparrow, and R. A. Magnuson, "Experiments on coupled parallel flows in a channel and a bounding porous medium," J. Basic Eng. **92**, 843 (1970).
[23]J. T. Jeong, "Slip boundary condition on an idealized porous wall," Phys. Fluids **13**, 1884 (2001).
[24]D. F. James and A. M. J. Davis, "Flow at the interface of a model fibrous porous medium," J. Fluid Mech. **426**, 47 (2001).
[25]M. F. Tachie, D. F. James, and I. G. Currie, "Velocity measurements of a shear flow penetrating a porous medium," J. Fluid Mech. **493**, 319 (2003).
[26]G. Neale and W. Nader, "Practical significance of Brinkman's extension of Darcy's law: Coupled parallel flow within a channel and a bounding porous medium," Can. J. Chem. Eng. **52**, 475 (1974).
[27]H. C. Brinkman, "A calculation of the viscous force exerted by flowing fluid on a dense swarm of particles," Appl. Sci. Res. **A1**, 27 (1947).
[28]T. Levy, "Loi de Darcy ou loi de Brinkman?" C. R. Acad. Sci. **292**, 872 (1981).
[29]D. A. Nield, "The limitation of the Brinkman–Forchheimer equation in modeling flow in a saturated porous medium and at an interface," Int. J. Heat Fluid Flow **12**, 269 (1991).
[30]A. Einstein, "Eine neue Bestimmung der Moleküldimensionen," Ann. Phys. **324**, 289 (1906); *Theory of the Brownian Movement* (Dover, New York, 1956).
[31]J. A. Ochoa-Tapia and S. Whitaker, "Momentum transfer at the boundary between a porous medium and a homogeneous fluid—I. Theoretical development," Int. J. Heat Mass Transfer **38**, 2635 (1995).
[32]J. A. Ochoa-Tapia and S. Whitaker, "Momentum transfer at the boundary between a porous medium and a homogeneous fluid—II. Comparison with experiment," Int. J. Heat Mass Transfer **38**, 2647 (1995).
[33]B. Goyeau, D. Lhuillier, D. Gobin, and M. G. Velarde, "Momentum transport at a fluid-porous interface," Int. J. Heat Mass Transfer **46**, 4071 (2003).
[34]P. Neogi and C. A. Miller, "Spreading kinetics of a drop on a rough solid surface," J. Colloid Interface Sci. **92**, 338 (1983).
[35]S. H. Davis and L. M. Hocking, "Spreading and imbibition of viscous liquid on a porous base," Phys. Fluids **11**, 48 (1999).
[36]V. M. Starov, S. R. Kosvintsev, V. D. Sobolev, M. G. Velarde, and V. G. Zhdanov, "Spreading of liquid drops over saturated porous layers," J. Colloid Interface Sci. **246**, 372 (2002).
[37]G. Bayada and M. Chambat, "On interface conditions for a thin film flow past a porous medium," SIAM J. Math. Anal. **26**, 1113 (1995).
[38]J. P. Pascal, "Linear stability of fluid flow down a porous inclined plane," J. Phys. D **32**, 417 (1999).
[39]J. P. Pascal, "Instability of power-law fluid flow down a porous incline," J. Non-Newtonian Fluid Mech. **133**, 109 (2006).
[40]S. Whitaker, "The Forchheimer equation: A theoretical derivation of Darcy's law," Transp. Porous Media **25**, 27 (1996).
[41]P. Bousquet-Melou, B. Goyeau, M. Quintard, F. Fichot, and D. Gobin, "Average momentum equation for interdendritic flow in a solidifying columnar mushy zone," Int. J. Heat Mass Transfer **45**, 3651 (2002).
[42]S. Whitaker, "Flow in porous media I: A theoretical derivation of Darcy's law," Transp. Porous Media **1**, 3 (1986).
[43]D. A. Nield and A. Bejan, *Convection in Porous Media* (Springer-Verlag, New York, 1999).
[44]A. A. Nepomnyashchy, M. G. Velarde, and P. Colinet, *Interfacial Phenomena and Convection* (CRC, Boca Raton, FL, 2002).
[45]M. Chandesris, "Modélisation des coulements turbulents dans les milieux poreux et á l'interface avec un milieu libre," Ph.D. thesis, Université de Paris 6, 2006.
[46]B. Scheid, A. Oron, P. Colinet, U. Thiele, and J. C. Legros, "Nonlinear evolution of nonuniformly heated falling liquid films," Phys. Fluids **14**, 4130 (2002).
[47]M. C. Cross and P. C. Hohenberg, "Pattern formation out of equilibrium," Rev. Mod. Phys. **65**, 851 (1993).
[48]T. B. Benjamin, "Wave formation in laminar flow down an inclined plane," J. Fluid Mech. **2**, 554 (1957).
[49]C. S. Yih, "Stability of liquid flow down an inclined plane," Phys. Fluids **6**, 321 (1963).
[50]U. Thiele, M. G. Velarde, and K. Neuffer, "Dewetting: Film rupture by nucleation in the spinodal regime," Phys. Rev. Lett. **87**, 016104 (2001).
[51]U. Thiele, L. Brusch, M. Bestehorn, and M. Bär, "Modelling thin-film dewetting on structured substrates and templates: Bifurcation analysis and numerical simulations," Eur. Phys. J. E **11**, 255 (2003).
[52]U. Thiele, M. G. Velarde, K. Neuffer, M. Bestehorn, and Y. Pomeau, "Sliding drops in the diffuse interface model coupled to hydrodynamics," Phys. Rev. E **64**, 061601 (2001).
[53]U. Thiele, J. M. Vega, and E. Knobloch, "Long-wave Marangoni instability with vibration," J. Fluid Mech. **546**, 61 (2006).
[54]U. Thiele and E. Knobloch, "On the depinning of a driven drop on a heterogeneous substrate," New J. Phys. **8**, 1 (2006).
[55]K. John, M. Bär, and U. Thiele, "Self-propelled running droplets on solid substrates driven by chemical reactions," Eur. Phys. J. E **18**, 183 (2005).
[56]A. Pototsky, M. Bestehorn, D. Merkt, and U. Thiele, "Morphology changes in the evolution of liquid two-layer films," J. Chem. Phys. **122**, 224711 (2005).
[57]A. Pereira, P. M. J. Trevelyan, U. Thiele, and S. Kalliadasis, "Dynamics of a horizontal thin liquid film in the presence of reactive surfactants," Phys. Fluids **19**, 112102 (2007).
[58]U. Thiele, S. Madruga, and L. Frastia, "Decomposition driven interface evolution for layers of binary mixtures: I. Model derivation and stratified base states," Phys. Fluids **19**, 122106 (2007).
[59]E. Doedel, H. B. Keller, and J. P. Kernevez, "Numerical analysis and control of bifurcation problems (I) Bifurcation in finite dimensions," Int. J. Bifurcation Chaos Appl. Sci. Eng. **1**, 493 (1991).
[60]E. Doedel, H. B. Keller, and J. P. Kernevez, "Numerical analysis and control of bifurcation problems (II) Bifurcation in infinite dimensions," Int. J. Bifurcation Chaos Appl. Sci. Eng. **1**, 745 (1991).
[61]E. J. Doedel, A. R. Champneys, T. F. Fairgrieve, Y. A. Kuznetsov, B. Sandstede, and X. J. Wang, "AUTO97, continuation and bifurcation software for ordinary differential equations," Concordia University, Montreal, 1997.
[62]U. Thiele and E. Knobloch, "Front and back instability of a liquid film on a slightly inclined plate," Phys. Fluids **15**, 892 (2003).
[63]W. Boos and A. Thess, "Cascade of structures in long-wavelength Marangoni instability," Phys. Fluids **11**, 1484 (1999).
[64]P.-G. de Gennes, "Wetting: Statics and dynamics," Rev. Mod. Phys. **57**, 827 (1985).